Biomaterials 34 (2013) 841–853

Contents lists available at SciVerse ScienceDirect

Biomaterials

journal homepage: www.elsevier.com/locate/biomaterials

The spatial and temporal control of cell migration by nanoporous surfaces through the regulation of ERK and integrins in fibroblasts

Hsu-An Pan [a,1], Jia-You Liang [a,1], Yao-Ching Hung [b,c], Chia-Hui Lee [a], Jin-Chern Chiou [d], G. Steven Huang [a,*]

[a] Department of Materials Science and Engineering, National Chiao Tung University, Hsinchu 300, Taiwan, ROC
[b] College of Medicine, China Medical University, Taichung 40402, Taiwan, ROC
[c] Department of Obstetrics and Gynecology, China Medical University Hospital, Taichung 40402, Taiwan, ROC
[d] Institute of Electrical Control Engineering, National Chiao Tung University, Hsinchu 300, Taiwan, ROC

ARTICLE INFO

Article history:
Received 17 July 2012
Accepted 29 September 2012
Available online 3 November 2012

Keywords:
Nanopores
Stainless steel
Cell migration
Focal adhesion
Integrins
ERK

ABSTRACT

Nanotopography controls cell behaviours, such as cell adhesion and migration. However, the mechanisms responsible for topology-mediated cellular functions are not fully understood. A variety of nanopores was fabricated on 316L stainless steel to investigate the effects of spatial control on the growth and function of fibroblasts, the temporal regulation of integrins, and their effects on migration. The NIH-3T3 fibroblast cell line was cultured on the nanopore surfaces, whose pore diameters ranged from 40 to 210 nm. The 40 and 75 nm nanopores enhanced cell proliferation, focal adhesion formation and protein expression of vinculin and β-tubulin after 24 h of incubation. Integrin expression was analysed by qPCR, which showed the extent of spatial and temporal regulation achieved by the nanopores. The protein expression of pERK1/2 was greatly attenuated in cells grown on 185 and 210 nm nanopore surfaces at 12 and 24 h. In summary, the 40 and 75 nm nanopore surfaces promoted cell adhesion and migration in fibroblasts by controlling the temporal expression of integrins and ERK1/2. The current study provides insight into the improvement of the design of stainless steel implants and parameters that affect biocompatibility. The ability to regulate the expression of integrin and ERK1/2 using nanopore surfaces could lead to further applications of surface modification in the fields of biomaterials science and tissue engineering.

1. Introduction

Cell migration plays a critical role in a variety of biological and disease processes such as the healing of skin, connective tissue repair and inflammation [1]. After tissue injury, fibroblasts migrate towards the wound, enhance cell division near the edge of the wound and secrete ECM to support further cell migration [2]. The presence of various types of fibroblasts is critical to wound recovery [3]. Therefore, controlling fibroblast migration and proliferation is essential to improving tissue repair processes after implantation. The mechanics of cell migration are ascribed to the focal adhesion between integrin and ECM. The fibronectin receptor α5β1 integrin is highly expressed in human fibroblasts and promotes fibroblast motility and survival [4]. Moreover, α11β1 is the major receptor for collagen I on mouse embryonic fibroblasts and might be required for cell migration [5]. The optimum speed of cell migration occurs at intermediate levels of expression of α5β1 or α2β1 integrins or intermediate concentrations of ligands, including fibronectin or collagen [6]. In addition, the activation of the extracellular signal-regulated kinase (ERK) is believed to direct cell migration, attachment and integrins expression [7]. Studies have shown that integrin α2 plays a critical role in mediating ERK activation for cell adhesion and motility [8]. ERK is activated during the formation of focal adhesions and the regulation of human corneal epithelial cell migration associated with wound closure [9].

The ability of cells to adhere, migrate and express cell functions on metallic surfaces is crucial for tissue repair after implantation. One of the prevailing metallic materials is 316L stainless steel because its favourable combination of strength, fabrication properties and low *in vivo* toxicity make it suitable for use in orthopaedic, dental and surgical implants [10]. Further, 316L stainless steel shows reduced cytotoxicity and inflammatory response through the regulation of lactate dehydrogenase activity and

* Corresponding author. Department of Materials Science and Engineering, National Chiao Tung University, 1001 University Road, EE137, Hsinchu 300, Taiwan, ROC. Tel.: +886 3 5131451; fax: +886 3 5729912.
E-mail address: gstevehuang@mail.nctu.edu.tw (G.S. Huang).
[1] These authors contributed equally to this work.

0142-9612/$ – see front matter © 2012 Elsevier Ltd. All rights reserved.
http://dx.doi.org/10.1016/j.biomaterials.2012.09.078

tumour necrosis factor alpha in human monocytes [11]. Therefore, stainless steel can provide an anti-corrosion and non-cytotoxic surface to induce the adhesion of osteoblasts [12]. A critical factor to consider in developing metallic biomimetic cell-stimulating cues is the fact that the extracellular environment features nano-scale topographic interfaces. However, only a few studies have discussed the cellular responses of molecules such as integrin on metallic surface topographies. The focus of this study is to combine fundamental aspects of nanotopography and cellular molecular biology to temporally modulate cell-substrate responses between NIH-3T3 fibroblasts and nanopore surfaces of 316L stainless steel.

Surface modification has been used to improve the biocompatibility of stainless steel implants. Enhanced human osteoblast cell adhesion and proliferation has been observed on 316L stainless steel after calcium phosphate or hydroxyapatite-coated treatment [13]. However, hydroxyapatite and calcium phosphate coatings with thicknesses of ~10–100 μm are chemically unstable and exhibit deteriorating mechanical strength during long-term implantation *in vivo* [14,15]. Nanotopography may hold the key to modifying the surfaces and enhancing the mechanical strength of metallic implants. Previous studies have shown that the surfaces of 30 nm TiO_2 nanotubes promote stem cell adhesion, whereas nanotubes measuring 70–100 nm induce cytoskeletal stress and differentiation into osteoblast-like cells [16]. Endothelial cells are able to interact with 100 nm TiO_2 nanotubes to achieve enhanced cellular migration, focal adhesion and viability [17]. Furthermore, nanotopography may regulate integrins expression and modulate cell function. Structures featuring 14 nm deep pits enhance osteoblastic cell attachment and spreading by enhancing integrin αV expression [18]. Integrin α2β1 signalling, required for osteoblastic differentiation, can be induced by the sub-microstructure of the Ti surface [19]. Although the molecular mechanism that governs the topological control of nanostructures over cell migration is under intensive investigation, the temporal expression of genes in adapting to a nanostructured environment has yet to be explored. Furthermore, the correlation between the entire spectrum of integrins expression and cellular migration when interacting with nanostructured surfaces requires systematic investigation.

To further explore the general phenomenon of topological sensing, experiments using the NIH-3T3 cell line were performed to investigate the nanotopological influence of different nanoscale structures [20]. In the current study, nanopores with diameters ranging from 40 to 210 nm were created on stainless steel. The effects on cell growth, migration, and adhesion were evaluated. In particular, the temporal expression of integrins was quantified. The aim of this study was to investigate the size dependence of nanopore surfaces on the growth and function of fibroblasts and to discuss the interplay between adhesion and migration, together with advanced surface nano-engineering, which might help us understand cellular responses to nano-environments.

2. Materials and methods

2.1. Cell culture

To eliminate the possible contamination of nano-microparticles, cell culturing was performed in a class-10 clean room. NIH-3T3 fibroblasts were cultured in Dulbecco's Modified Eagle's Medium without antibiotics and were complimented with 10% FCS. The cells were incubated at 37 °C in 5% CO_2.

2.2. Chemicals

Glutaraldehyde and osmium tetroxide were purchased from Electron Microscopy Sciences (USA). Anti-vinculin mouse antibody was purchased from Abcam (USA). Alexa Fluor 594 phalloidin and Alexa Fluor 488 goat anti-mouse IgG were purchased from Invitrogen (USA). Trypsin was purchased from Sigma (USA). Bromodeoxyuridine and antibody were purchased from Millipore. Other chemicals of analytical grade or higher were purchased from Sigma or Merck. Anti-integrin rabbit antibody and anti-β-tubulin mouse antibody were purchased from Novus.

2.3. Fabrication of nanopore surfaces

Medical 316L stainless steel samples were mechanically polished with abrasive papers (grade 250, 800, 2000 and 4000) followed by alumina powder (0.3 μm). Electropolishing was then executed in an electrolytic bath, whose temperature was maintained between 5 and 10 °C for 30 min. The electrolyte was composed of a mixture of 40 mL of perchloric acid and 760 mL of ethylene-glycol monobutylether [21]. The applied voltages for anodisation were 30, 45, 60, 70, and 75 V for 40, 75, 160, 185, and 210 nm nanopore surfaces, respectively; the electrolytic solution was stirred by a rotating magnet. After electropolishing, the samples were rinsed with large amounts of distilled water and then cleaned with the electrolyte overnight. Polished stainless steel substrates were used as control flat substrates. Five flat nanopore surfaces ($n = 6$) were analysed by scanning electron microscopy (JEOL JSM-6500 TFE-SEM). Atomic force microscopy (AFM) was used to characterise the depths and roughness of the substrates.

2.4. Morphological observation by scanning electron microscopy (SEM)

Fibroblasts were seeded at a density of 5.0×10^3 cells/cm^2 on the different nanopore surfaces for 12, 24, 48 and 72 h of incubation. After removing the culture medium, the wells were rinsed three times with phosphate buffer saline (PBS). The cells were fixed with 1% glutaraldehyde in PBS at 4 °C for 20 min, followed by post-fixation in 1% osmium tetroxide for 30 min. Dehydration was performed using a series of ethanol concentrations (10 min incubation each in 50%, 60%, 70%, 80%, 90%, 95%, and 100% ethanol), after which the samples were air dried. The specimens were sputter-coated with platinum and examined by JEOL JSM-6500 TFE-SEM at an accelerating voltage of 5 kiloelectron volts (keV). The surface area of the cells grown on nanopores was quantified and compared to the surface area of cells grown on a flat surface using the ImageJ software package (NIH) to trace the cytoplasmic borders of the cells. SEM images of six different substrate fields were measured per sample, and three separate samples were measured for each nanopore surface.

2.5. Measurement of cell number by cell density

Cells were double stained using 4′,6-diamidino-2-phenylindole (DAPI) and phalloidin. NIH-3T3 fibroblasts were harvested and fixed using 4% paraformaldehyde diluted in PBS for 30 min, followed by three washes in PBS. Cell membranes were permeabilised during a 10 min incubation in 0.1% Triton X-100, followed by three PBS washes. MG63 cells were incubated with phalloidin and nuclei counterstained with DAPI for 15 min at room temperature. The samples were mounted and imaged using a Leica TCS SP2 confocal microscope. The cell number was counted using the ImageJ software package and expressed in terms of cell

Table 1
Gene names and sequence primers for real-time PCR.

Gene	Forward sequence	Reverse sequence
GAPDH	tcttcaccaccatggagaagg	ctcactggcatgaccttc
β1-integrin	gaggttcaatttgaaattagc	ggctctgcactgaacacattc
β2-integrin	aggagcatcgctaatcctga	ccagactcggtgatctcgtt
β3-integrin	ggacatctactacttgatgg	accgtgtctccaatcttgag
β4-integrin	agggaggctggctttcaatgtagt	ttcaccaggtgctcagtgtcatca
β5-integrin	tatgcactagtggaagtgcc	ccctcacacttcctctgacc
β6-integrin	tctgacattgttcagattgc	acttccagttccacctcaga
β7-integrin	agtgtgcgactgtaactgtggtga	actctgcacaatccctgtactgct
β8-integrin	caaaggacagtgtgcggaag	gttgacacagtgctgtgctg
α1-integrin	cgatgacgctctgccaaact	ccgaagttctggcattggga
α2-integrin	gcaccacattagcatacaga	ggcatcatacaggagaggaa
α3-integrin	gtctggaaaccttgtcaaccc	caaccacagctcaatctcagc
α4-integrin	cccaggctacatcgttttgt	ccatgctaatcccagtgtt
α5-integrin	ctgcagctgcatttccgagtctgg	gaagccgagcttgtagaggacgta
α6-integrin	tggaggtacagttgttggtgagca	aaacaccgtcactcgaacctgagt
α7-integrin	ccaggacctggccatccgtg	ctatccttgcgcagaatgac
α8-integrin	gcccagcttctgctgcaccg	cccaaggtcacacaccacca
α9-integrin	cctaacgttgcactgcaacc	agcagaaaaatgaggatcccc
α10-integrin	tggagtctctctccatcc	tcgatgaacagtcttcctaccagc
α11-integrin	ccgccttcctctgcttcataccca	gccgcctctcctcgttcacacacact
αIIb-integrin	tggtggtggcagcagaagaa	gtagggaggagacgttgaac
αD-integrin	tggatctcgactcgtggtgg	cacttttcgggccccattc
αE-integrin	ggacgatcaagcaacatcaa	ggaaccgtgctcattaaagg
αL-integrin	ttgagggcacaaacagacag	tcatccaggccacagtgtaa
αM-integrin	cagatcaacaatgtgaccgtatgg	catcatgtccttgtactgccgc
αV-integrin	gtcttatacagagccagacccg	cttcacagtcagtgtcagaggg
αX-integrin	acacagtgtgctccagtatga	gcccagggatatgttcacagc

density. Six different substrate fields were measured per sample, and three separate samples were measured for each nanopore surface.

2.6. Immunostaining

Fibroblasts were seeded at a density of 5.0×10^3 cells/cm^2 on the different nanopore surfaces for 12, 24, 48 and 72 h of incubation. The adhered cells were fixed with 4% paraformaldehyde in PBS for 15 min followed by three PBS washes. The cell membranes were permeated by incubating in 0.1% Triton X-100 for 10 min, followed by three PBS washes, and were then blocked by 1% BSA in PBS for 1 h, followed by an additional three PBS washes. The samples were incubated with phalloidin and anti-vinculin antibody, which was diluted in 0.5% BSA for 1 h, followed by incubating with Alexa Fluor 488 goat anti-mouse antibody for 1 h, three PBS washes and examination using a Leica TCS SP2 confocal microscope. Immunostaining with anti-vinculin antibody and phalloidin as performed. The focal adhesion area and number per cell were determined using ImageJ. For each experimental condition, the number of vinculin plaques and microfilament bundles per cell were counted and compared to those for cells that were cultured on a flat surface.

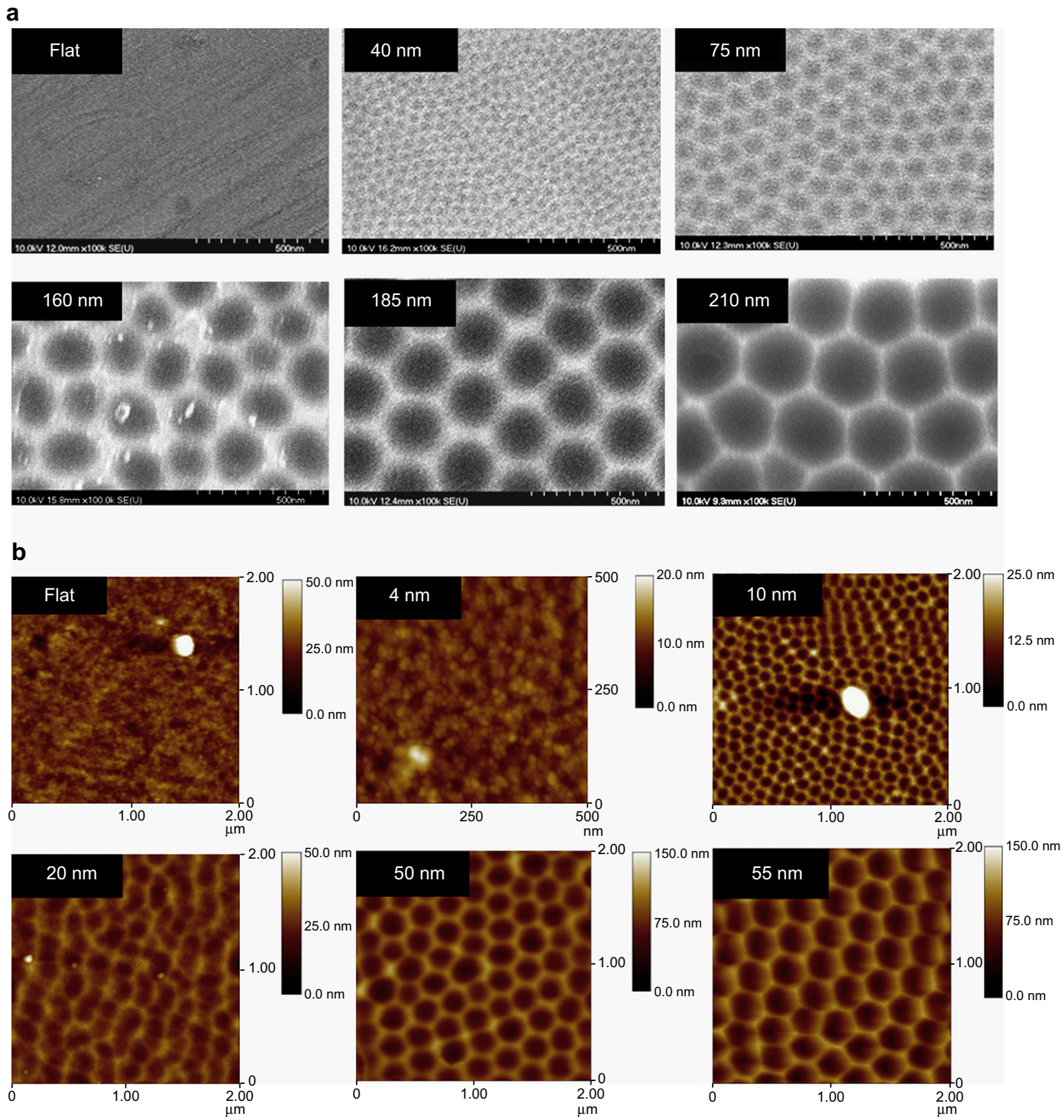

Fig. 1. Surfaces of highly ordered nanopores with different diameters on 316L stainless steel. (a) SEM images showing highly ordered nanopores of five different sizes between 40 and 210 nm that were fabricated by varying the anodisation potential from 30 to 75 V. Scale bar = 500 nm (b) AFM images showing nanopore surfaces with pore depths of 4, 10, 20, 50 and 55 nm.

Table 2
Characteristic surface parameters.

	Flat	Nanopore (nm)				
		40	75	160	185	210
Diameter (nm)	–	38.4 ± 5	73 ± 7	157 ± 12	185 ± 15	210 ± 14
Depth (nm)	–	4.2 ± 0.8	9.8 ± 1	22 ± 2	52 ± 7	54 ± 2.6
Pitch (nm)	–	23 ± 3	32 ± 3	44 ± 4	47 ± 5	50 ± 4
Mean roughness (nm)	0.5 ± 0.2	0.2 ± 0.1	0.6 ± 0.2	0.7 ± 0.14	3 ± 0.3	2.3 ± 1.5
Maximum roughness (nm)	2.5 ± 0.9	0.96 ± 0.3	3.3 ± 1	3.9 ± 1.5	15 ± 2.3	16 ± 9

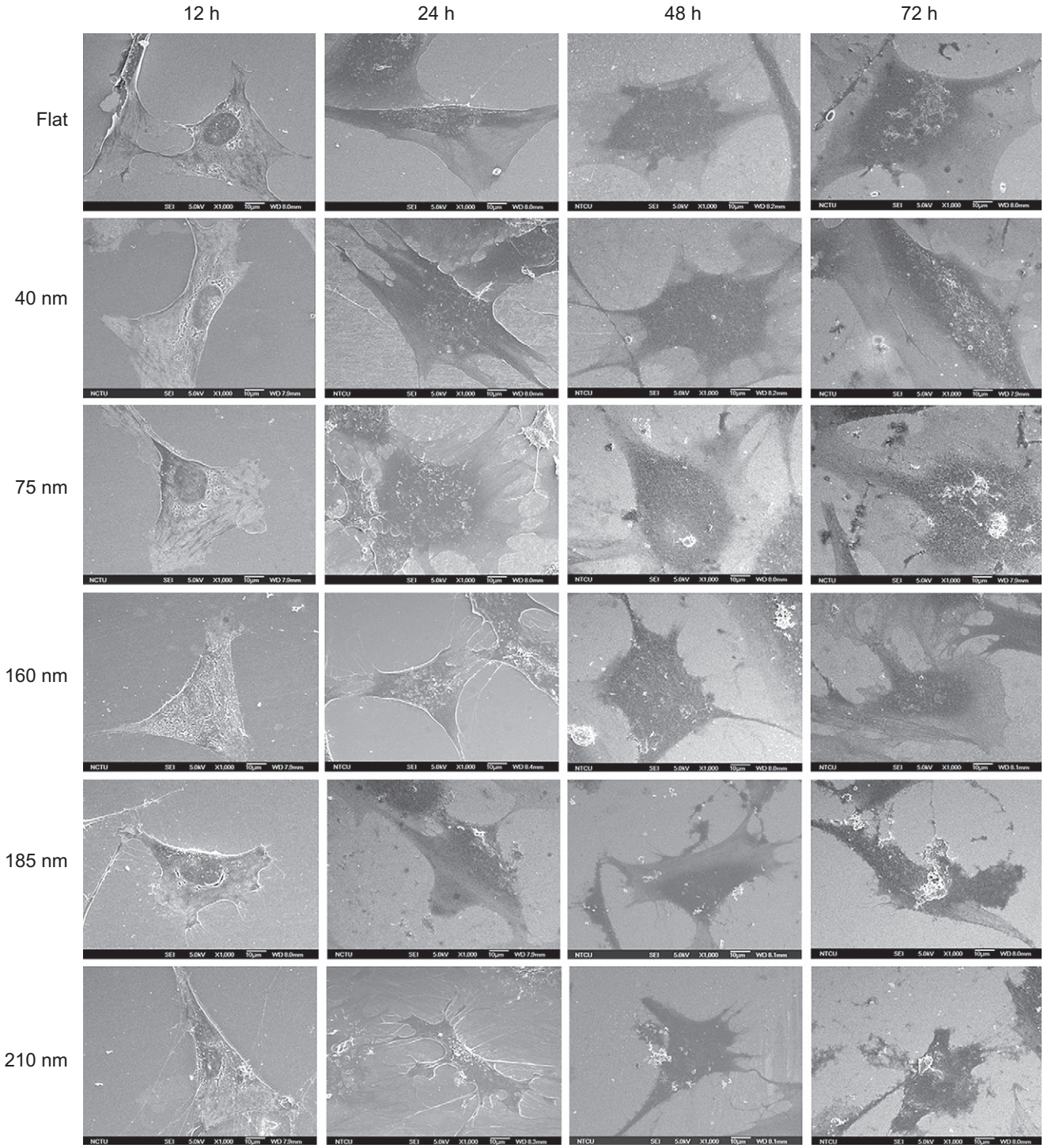

Fig. 2. The morphology of NIH-3T3 fibroblasts seeded on nanopore surfaces. Fibroblast growth on flat, 40 nm, 75 nm, 160 nm, 185 nm and 210 nm nanopore surfaces and their morphologies were observed by SEM after 12, 24, 48 and 72 h of incubation. Scale bar = 10 μm.

2.7. Quantitative real-time PCR

Oligo primers used to amplify genes of interest were designed based on the sequences provided in previous reports [22] (Table 1). The specificity of the synthesised primers was verified by polymerase chain reaction (PCR) using reverse transcribed mRNA extracted from an NIH-3T3 fibroblast as a template. The sizes of the PCR products were resolved using agarose gel electrophoresis. Total RNA was extracted by using TRI-reagent (Talron Biotech) according to the manufacturer's specifications. The RNA was isolated using chloroform extraction and isopropanol precipitation. The RNA extract was immediately purified using an RNeasy Mini Kit (Qiagen) to remove impurities and unwanted organic compounds. Purified RNA was resuspended in DEPC-treated water and quantified by OD_{260}. The OD_{260}-to-OD_{280} ratio usually exceeded 2.0 at this stage. For cDNA synthesis, 1 μg total RNA was annealed using 1 μg oligo-dT primer, followed by reverse transcription using SuperScript® III Reverse Transcriptase (Invitrogen) in a total volume of 50 μL. Between 0.2 and 0.5 μL of the reverse transcription reactions were used for quantitative PCR using SYBR Green I performed on an iCycler iQ5 (Bio-Rad Laboratories). The cycling conditions were as follows: 1 cycle of 5 min at 95 °C and 50 cycles of 20 s at 95 °C, 20 s at 55 °C, and 40 s at 72 °C. Fluorescence was measured after each 72 °C step. The expression levels were obtained using threshold cycles (Ct) that were determined by the iCycler iQ Detection System software. Relative transcript quantities were calculated using the ΔΔCt. GAPDH was used as a reference gene and was amplified along with the target genes from the same cDNA samples. The difference in threshold cycles between the sample mRNA and GAPDH mRNA was defined as the ΔCt. The difference between the ΔCt of the control cells and the ΔCt of the cells grown on nanopore surfaces was defined as the ΔΔCt. The fold change in mRNA expression was expressed as $2^{\Delta\Delta Ct}$. The results were expressed as the mean ± SD of six experiments.

2.8. Western blot

Cultured NIH-3T3 fibroblasts were lysed and centrifuged at 12,000 g for 2 min at 4 °C. The supernatants were transferred to new Eppendorf tubes and protein concentrations were defined by using UV/VIS spectroscopy. After the protein concentrations were defined, solutions were mixed with 4X sample buffer and lysis buffer to a final concentration of 1 mg/mL protein. Samples were heated at 95 °C for 3 min and cooled at 0 °C for 3 min; this step was repeated twice. Proteins were separated using 10% SDS-PAGE gels and transferred to PVDF membranes. Nonspecific protein binding was blocked using a 5% milk solution at 4 °C overnight. The membranes were subsequently blotted at 4 °C overnight using the specific antibodies indicated for each experiment, which were diluted in blocking buffer. Specific primary antibodies were blotted using second antibodies in the blocking buffer at room temperature for 1 h. Chemiluminescent detection was performed using western blotting luminol and oxidising reagents (USA.).

2.9. Wound healing assay

To conduct a wound healing assay, 1×10^5 cells were grown on the nanopore surfaces and allowed to reach confluence and further incubated in medium containing 2% FCS. The cell monolayers were wounded by a plastic pipette [23]. After wounding, cells were washed with PBS and incubated for 6, 12, 18, 24 and 48 h in medium containing 2% FCS. After incubation, the cells were fixed with 4% paraformaldehyde in PBS for 30 min, followed by three PBS washes. The cell membranes were permeated by incubating in 0.1% Triton X-100 for 10 min, followed by three PBS washes. The samples were incubated with DAPI and phalloidin for 15 min at room temperature, followed by three PBS washes. Images of cell samples were taken with a fluorescence microscope. The areas between the cell layer borders were measured. Cell numbers in the wounding region were calculated using fluorescence images.

2.10. Statistics

The experiments were repeated three times on the nanopore surfaces. Data were expressed as the mean ± standard deviation. A one-way analysis of variance followed by Tukey's post test was used for statistical analysis (GraphPad, La Jolla, CA), and the level of significance was set to $P < 0.05$.

3. Results

3.1. Fabrication of nanopore surfaces

Nanopores with pore diameters of 40, 75, 160, 185 and 210 nm were fabricated as described above, by electropolishing on 316L stainless steel. After electropolishing, the morphology, depth and roughness of the surfaces was verified by SEM and AFM images (Fig. 1). Highly ordered nanopores with 5 different pore sizes between 40 and 210 nm were created. Polished stainless steel substrates were used as control flat substrates. The characteristic parameters are outlined in Table 2. The pore depths were 4, 10, 20, 50 and 55 nm for pore sizes of 40, 75, 160, 185 and 210 nm, respectively. The surface roughness of the nanopores increased with the applied voltage. The nanopore surfaces were well controlled and highly defined.

3.2. Nanopore-modulated cell morphology and growth of fibroblasts

Nanotopography is known to modulate the cell morphology of NIH-3T3 fibroblasts [24]. To evaluate the growth of fibroblasts, NIH-3T3 fibroblasts were cultured on nanopores and flat 316L stainless steel substrates for 12, 24, 48 and 72 h. SEM images showed that the cells seeded on 40 and 75 nm nanopore surfaces exhibited extended morphology, with a large cell spreading areas. However, the cells seeded on 185 and 210 nm nanopore surfaces were smaller with restricted lamellipodia (Fig. 2). The cell spreading area was measured and compared with that of cells grown on flat surfaces. The maximum spreading area was observed for cells grown on 40 and 75 nm nanopores (Fig. 3a).

The size-dependent modulation of cells by nanopores was investigated over different culture times. Viable cells were counted

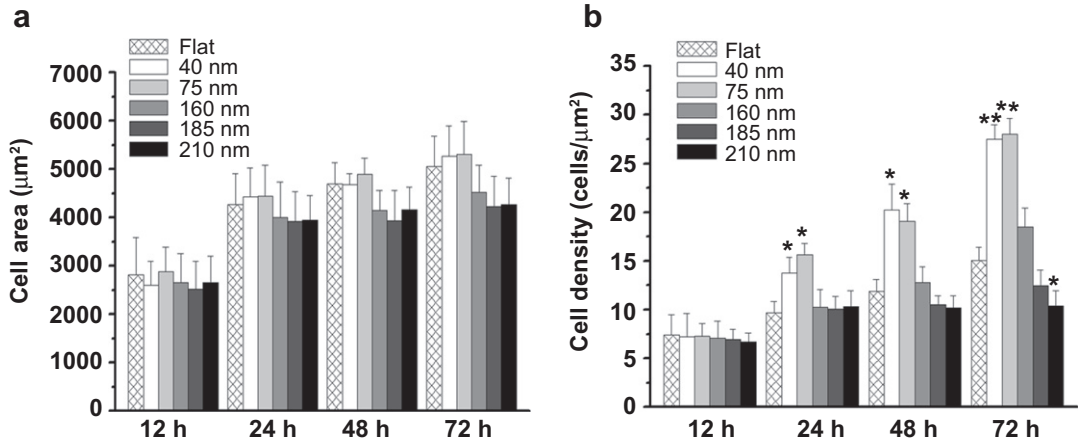

Fig. 3. The spreading area and density of NIH-3T3 fibroblasts attached to the different nanopore surfaces. Fibroblasts seeded on nanopore surfaces of various sizes were harvested after 12, 24, 48 and 72 h of culture. (a) Histogram of the cell spreading area, and (b) the cell density on different sizes of nanopores. The cell spreading area and density were defined using SEM images of 50 cells per condition. The mean ± SD from at least 3 experiments is shown. $^*p < 0.05$ and $^{**}p < 0.01$ when compared with flat control surfaces.

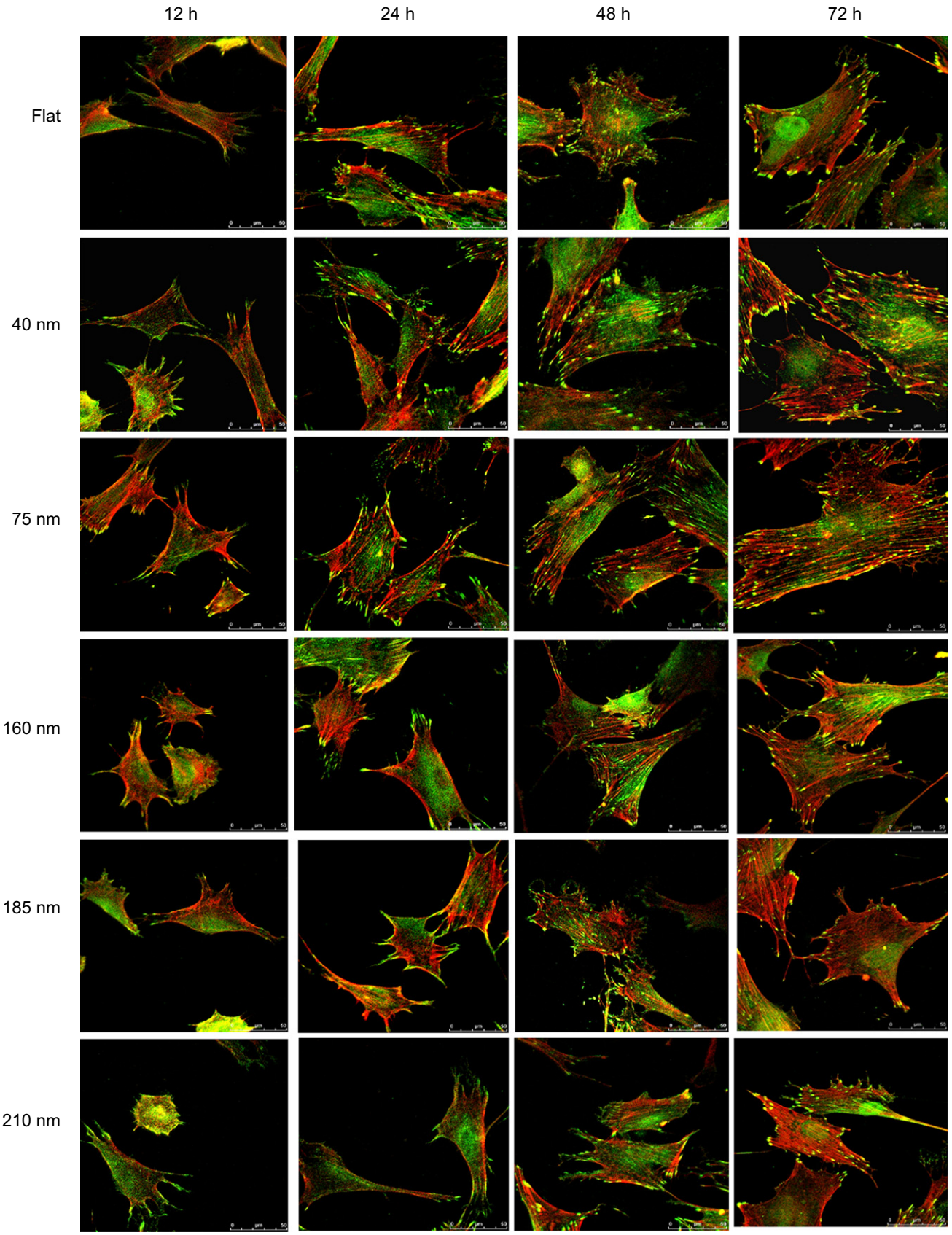

Fig. 4. Fluorescent images showing focal adhesion formation through vinculin (green) and actin filaments (red). NIH-3T3 fibroblasts were seeded on flat, 40 nm, 75 nm, 160 nm, 185 nm and 210 nm nanopores for 12, 24, 48 and 72 h. The distribution of vinculin and actin filaments in the fibroblast cultured on the various nanopore surfaces was observed. Scale bar = 50 μm. (For interpretation of the references to colour in this figure legend, the reader is referred to the web version of this article.)

and compared to cells grown on flat surfaces (Fig. 3b). The cells grown on 40 and 75 nm nanopores surfaces started to outgrow after 24 h of incubation. A two-fold enhancement in cell number relative to the cell number on the flat substrates was observed on the 40 and 75 nm nanopore surfaces after 48 and 72 h of incubation, respectively. It should be noted that a slight but significant decrease in density was observed for cells grown on the 210 nm nanopore surface after 72 h. These results indicate that the diameter of the nanopores is a predominant factor in the stimulation of cell morphology and growth.

3.3. Nanopore-modulated cell adhesion and cytoskeleton of fibroblasts

Vinculin bridges focal adhesion complexes with cytoskeleton [25]. To evaluate the role of adhesion molecules in nanopore-induced cell attachment, immunostaining specific to vinculin was performed (Fig. 4). Vinculin staining was widely distributed within cells grown on flat surfaces and the 40 and 75 nm nanopore surfaces at 48 and 72 h. The amount of vinculin increased in cells grown on the flat surfaces and the 40 and 75 nm nanopore surfaces but decreased in cells grown on the 185 and 210 nm nanopore surfaces after 24, 48 and 72 h.

The number of focal adhesions (focal point density) and vinculin-stained area per cell were plotted against incubation time (Fig. 5a, b). Significant differences were observed after 24 h. At 48 h, cells grown on the 40 and 75 nm nanopore surfaces showed a significant increase in focal point density per cell. It should be noted that a slight but significant decrease in vinculin-stained area was observed for cells grown on the 210 nm nanopore surface at 48 h. Differences in focal point density and vinculin-stained area were more enhanced at 72 h. The average area and number of vinculin plaque decreased in cells grown on the 185 and 210 nm nanopore surfaces at 48 and 72 h. Overall, the 40 and 75 nm nanopore surfaces enhanced cell attachment. Nanopores measuring 185 and 210 nm in diameter reduced the formation of focal adhesions in fibroblasts.

Cytoskeleton plays a very important role in determining cell motility and shape. The tight cytoskeleton arrangement observed in this study was enhanced in cells grown on 40 and 75 nm nanopores but gradually disappeared in cells grown on the 160, 185 and 210 nm nanopore surfaces at 48 and 72 h (Fig. 4). The number of microfilament bundles per cell was calculated. At 48 and 72 h, cells grown on the 40 and 75 nm nanopore surfaces showed a significant increase in the number of microfilament bundles per cell. A decrease in the number of microfilament bundles was observed in cells grown on 185–210 nm nanopores at 48 and 72 h (Fig. 5c). Overall, well-organised actin filaments were visible in cells grown on the 40 and 75 nm nanopore surfaces. Nanopores measuring 160, 185 and 210 nm in diameter retarded the organisation of the cytoskeleton. Therefore, focal adhesion and cytoskeletal organisation was modulated by the feature size of the nanopore surfaces.

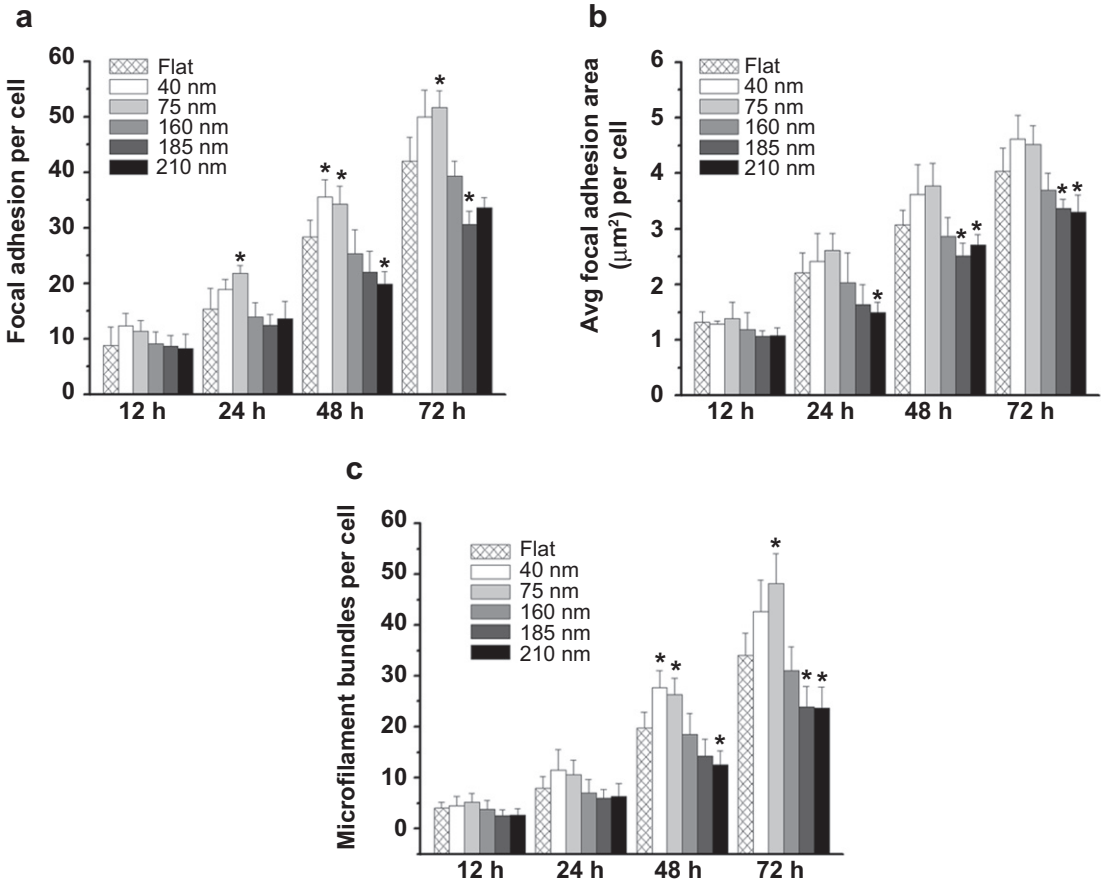

Fig. 5. The quantitative analysis of focal adhesion and cytoskeleton organisation on the nanopore surfaces. (a) The average number of vinculin plaques per cell cultured on different surfaces. (b) The average area of vinculin plaques per cell. (c) The average number of microfilament bundles per cell was calculated by F-actin fibre staining. The average adhesion number, vinculin plaque area and number of microfilament bundles were determined using fluorescent immunocytochemistry images of 50 cells per condition. The mean ± SD from at least 3 experiments is shown. $^{*}p < 0.05$ and $^{**}p < 0.01$ when compared with flat control surfaces.

3.4. Integrins expression of fibroblasts on various nanopore surfaces

Integrins serve as major receptors for ECM proteins, which play an essential role in cell migration, adhesion and proliferation [26]. Following the observation of the significant effect of nanopores on fibroblast viability, morphology and adhesion, a quantitative PCR (qPCR) was performed to analyse the temporal expression of the integrin gene family (Fig. 6). Fold expression levels were normalised against the expression levels observed for cells grown on flat surfaces. Cluster analysis was performed to find genes with similar expression patterns. As shown in Fig. 6, fibroblasts cultured on 40 and 75 nm nanopore surfaces showed similar integrin expression patterns at 12 h. However, the patterns changed at 24 and 48 h and switched to distinctive patterns at 72 h. The integrin expression patterns of cells grown on 160 and 185 nm nanopores also showed a similar state at 12 and 24 h. Furthermore, the expression of integrins (such as α2, α4, α6, α7, αV and β3) was up-regulated on the 75–210 nm nanopore surfaces at 48 h. The temporal expression of integrins was demonstrated.

After 12 h of cells culturing, the up-regulation of gene expressions for the integrins α1, α2, α9, α11, αIIb, β3 and β8 was obtained on the 40 and 75 nm nanopore surfaces. At 24 h, the integrins α1, α5, α7, α11, β6 and β8 showed up-regulation on 40 nm nanopores, and the integrins α1, α8, α9, α11, β5, β7 and β8 showed the same performance on the 75 nm nanopore surface. At 72 h, increased gene expression for the integrins α1, α6, αL, β1, β3 and β4 were observed on the 40 nm nanopore surface, and the expression of integrin α1, α4, αD, αL, β3 and β4 expression on the 75 nm nanopore surface was similar to that on the 40 nm nanopore surface. According to real-time PCR results, the gene expression of α2 and β3 was clearly higher on the 40 and 75 nm nanopore surfaces than on the other surfaces at 12 h. We also observed significant variations in the expression of α2, α9, α11, β3 subunits and β6 on the 40 and 75 nm nanopore surfaces at each point in time. For instance, α2 and β3 subunits were highly expressed on the 40 and 75 nm nanopore surfaces at 12 h but were down-regulated at 24 h. This finding suggests that both the nanopore surface structure and cell incubation time might be able to modulate integrin expression and regulate cell behaviour.

3.5. Protein expression of genes associated with cell adhesions

Western blots were performed to validate the expression of genes associated with cell adhesion and cytoskeleton. Protein expressions of vinculin, β-tubulin, integrin αV and integrin α2 were obtained after 12, 24 and 72 h of culturing (Fig. 7a). Protein expressions were quantified using GAPDH as a control and compared to those of cells grown on flat surfaces. For cells grown on the 40 and 75 nm nanopore surfaces, the expression of vinculin remained unchanged within 12 h, whereas it increased rapidly at 24 and 72 h (Fig. 7b). For the 185 and 210 nm nanopores surfaces, vinculin was down-regulated at 72 h relative to the vinculin activity observed in cells grown on a flat surface.

β-tubulin performs various vital cellular functions to support cell shape, migration and signal transduction [27]. After 12 h of culturing, β-tubulin exhibited stable expression on each nanopore surface (Fig. 7c). β-tubulin expression on the 40 and 75 nm nanopore surfaces showed up-regulation at 24 h. On the 185 and 210 nm nanopore surfaces, the expression was down-regulated at 72 h.

Integrin αV expression remained constant for all cultures at 12 and 24 h (Fig. 7d). Up-regulation of integrin αV was observed for cells grown on the 40, 75 and 160 nm nanopore surfaces at 72 h. For integrin α2, up-regulation was observed on the 75 nm nanopore surface at 12 h. After 24 h of culturing, a higher production of integrin α2 was observed for cells grown on the 185 and 210 nm nanopore surfaces (Fig. 7e). The temporal and spatial expression of

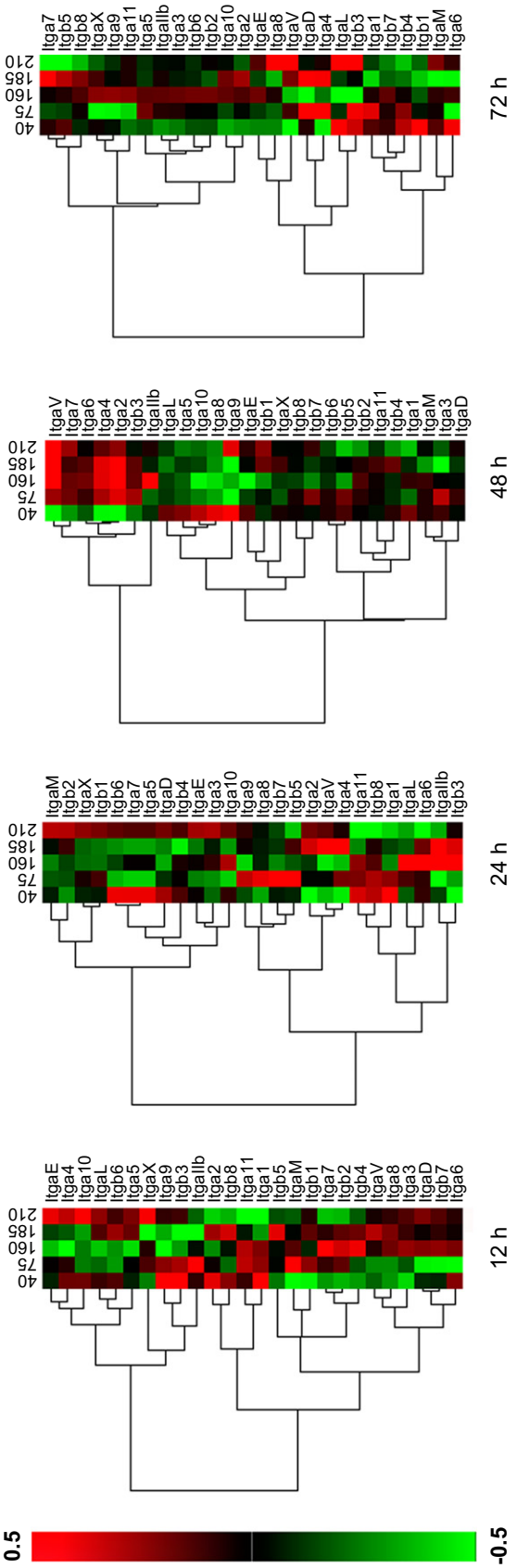

Fig. 6. The hierarchical cluster analysis of the real-time PCR data for integrin expression on different pore sizes between 40 and 210 nm at 12, 24, 48 and 72 h. The colour displays are (1) red when the gene is up-regulated relative to the control, (2) green when the gene is down-regulated relative to the control and (3) black when the difference is close to zero. The scale bar and colour values denote ± 0.5 standard deviation for each gene (row). Each value is the average of three experiments. (For interpretation of the references to colour in this figure legend, the reader is referred to the web version of this article.)

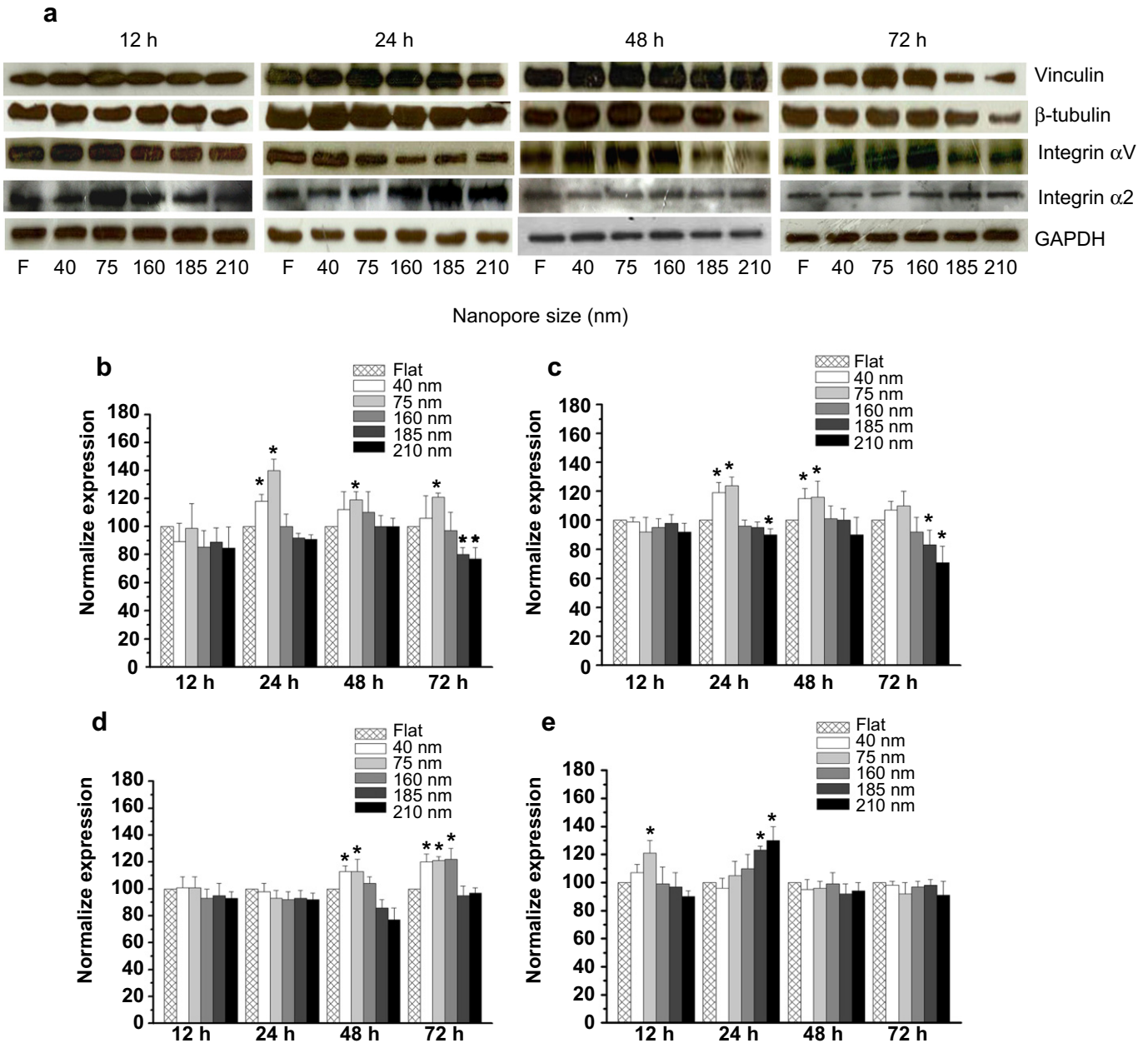

Fig. 7. Protein express in NIH-3T3 fibroblasts on nanopore surfaces. (a) The western blot pattern of vinculin, β-tubulin and integrins after culturing on nanopore surfaces for 12, 24, 48 and 72 h. The densitometry analysis of each band was performed and calculated using GAPDH expression as a control. We normalised (b) vinculin, (c) β-tubulin, (d) integrin αV, (e) and integrin α2 levels versus nanopore size. The mean ± SD from at least 3 experiments is shown. $^{*}p < 0.05$ when compared with flat control surfaces.

integrins derived from western blotting was consistent with those obtained by qPCR.

In addition, the activation of ERK is considered to direct cell migration, attachment and integrins expression. The expression of phosphorylated ERK1/2 (pERK1/2) was up-regulated in fibroblasts grown on the 40–160 nm nanopore surfaces at 48 h (Fig. 8a). In contrast, the expression of pERK1/2 was greatly attenuated in cells grown on the 185 and 210 nm nanopore surfaces at 12 and 24 h. After 72 h of culturing, the expression of pERK1/2 on the 160 and 185 nm nanopore surfaces was up-regulated (Fig. 8b).

3.6. Validation of migration by wound healing experiment

The surface properties of a material affect a cell's capability for movement, which must be preserved for successful implantation. Many studies on the structure of artificial implants enabling cell migration are important to making sure that cells can operate in a dynamic environment [28]. To further investigate the impact of nano-patterned structures on the function of fibroblasts, a wound healing assay was performed. Confluent cell monolayers were cultured on nanostructures for 12 h, wounded, and cultured for 6, 12, 18, 24 and 48 h. After 6 h of culturing on 40 and 75 nm nanopore surfaces, fibroblasts began to migrate into the wounded area at 6 h. At 12 and 18 h, the number of migrating cells was higher on the 40 and 75 nm nanopore surfaces than on the other surfaces. No differences were observed among all nanopore surfaces at 24 h (Fig. 9a). The number of migrating cells was calculated and compared with the counts obtained for a flat surface (Fig. 9b). The cell densities in the wounded area were similar on each nanopore surface at 6 h. After 12 h, the cells started to migrate into the

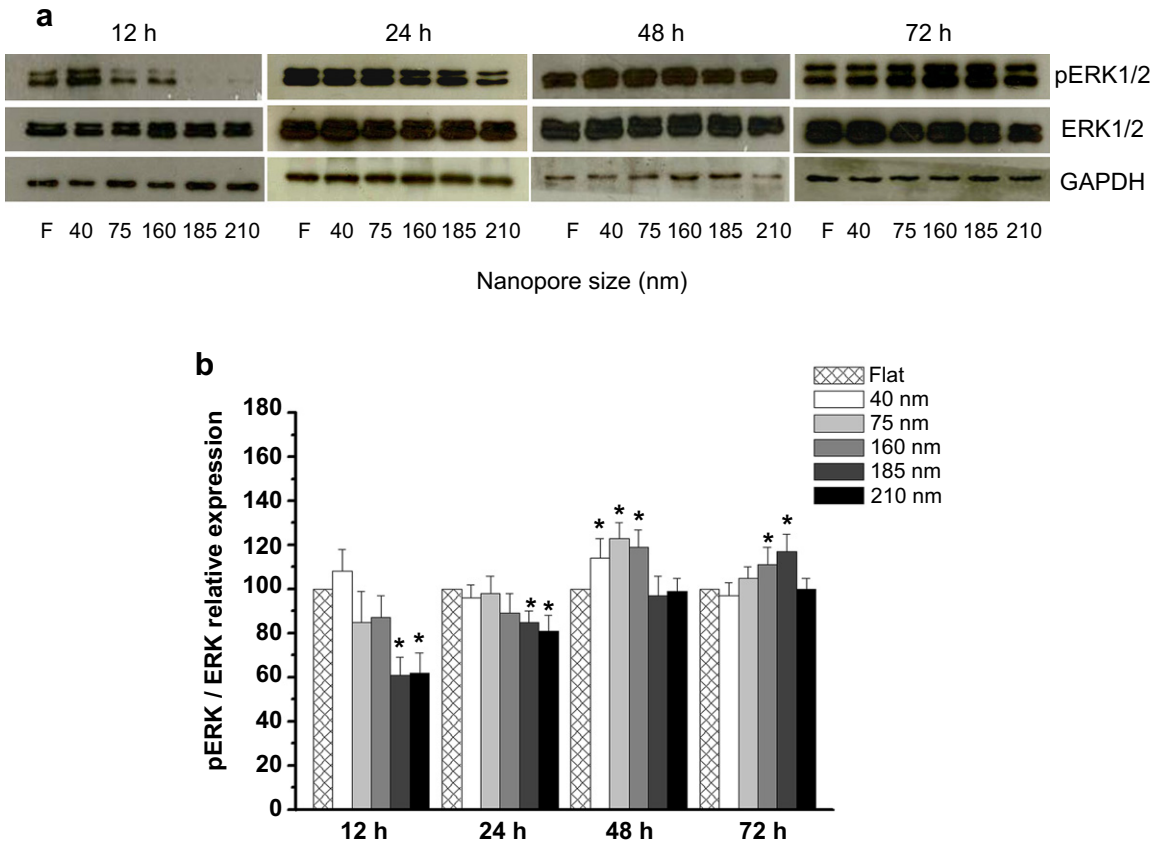

Fig. 8. Phosphorylation of ERK1/2 stimulated by nanopore surfaces. (a) The western blot pattern of phosphorylated ERK1/2 (pERK1/2) and total ERK1/2 (ERK1/2) after culturing on nanopore surfaces for 12, 24, 48 and 72 h. (b) The intensity of the phosphorylated ERK1/2 bands was determined by densitometry and normalised by that of the corresponding total ERK1/2 bands. The mean ± SD from at least 3 experiments is shown. $^{*}p < 0.05$ when compared with flat control surfaces.

wounded area. At 12, 18 and 24 h, significant cell migration was observed for the 40 and 75 nm nanopores surfaces with the increase in the density of migrating fibroblasts. The observed cell movement did not vary between cells grown on a flat surface and those grown on the 160, 185 and 210 nm nanopore surfaces at each time point. After 48 h, the cells migrated into the wounded region and formed a cell monolayer on each nanopore surface. These results suggest that the migration of NIH-3T3 fibroblasts could be modulated by nanopore surfaces and the duration of the culture period.

4. Discussion

Focal adhesion, cell spreading and subsequent proliferation are closely related to the surface characteristics of roughness and geometry [29]. The detailed mechanics through which the geometry and size of pores enhance cell attachment and proliferation are still unclear. An important question is whether a nanometre-scale adhesive unit exists, defined in terms of distance and number, that supports spreading. Our data indicate a positive correlation between decreasing pore size and increasing cell adhesion. The maximum focal point density and best organisation of cytoskeleton were observed in cells cultured on the 40 and 75 nm nanopore surfaces, whereas those cultured on the 160, 185 and 210 nm nanopore surfaces showed a reduction in the formation of focal adhesions and organisation of actin filaments. One possible mechanism through which nanopores may affect cell adhesion is by fostering an interaction between integrin anchoring sites and the edges of pores for cell attachment. Previous reports have shown that focal adhesion is enhanced when cells are cultured on pore surfaces with critical feature sizes smaller than 50 nm [30]. When adhesive dots are separated by >73 nm, the focal adhesions that are formed are aberrant, whereas separations of <58 nm between the dots allows for the effective formation of adhesions [31]. The negative cellular response to anchor spacings greater than 70 nm is ascribed to a lack of effective integrin clustering, which therefore inhibits the formation of focal adhesions and actin fibre networks [32]. Cell adhesion on different geometric structures revealed a significant increase in adhesion efficiency when integrin anchoring sites were spaced within 60 nm [33]. It was concluded that nanopores may induce nanoscale differences in anchor integrin density to affect the assembly of adhesion sites. Furthermore, the roughness of nanopores may be implicated in regulating cell adhesion. The rough topographical structures are capable of exerting positive and negative influences on cell adhesion and proliferation [34]. Nanopores measuring 40, 75 and 160 nm also provide smaller roughness to induce cell focal adhesion and proliferation. These phenomena suggest that the cellular responses are clearly modulated by nanopore features in a size-dependent manner.

Integrins belong to a major family of promigratory receptors that support adhesion to the ECM, stabilise protrusions through structural connections to the cytoskeleton, and activate migration-related signalling molecules [6]. Integrin-controlled cell adhesion is preferentially mediated by α5β1, αvβ3 and α2β1 [35]. Recent studies have indicated that integrin expression is greatly perturbed on nanopore surfaces with feature diameters between 70 and 300 nm [36], indicating that the integrins β1, β5, α5 and αV are

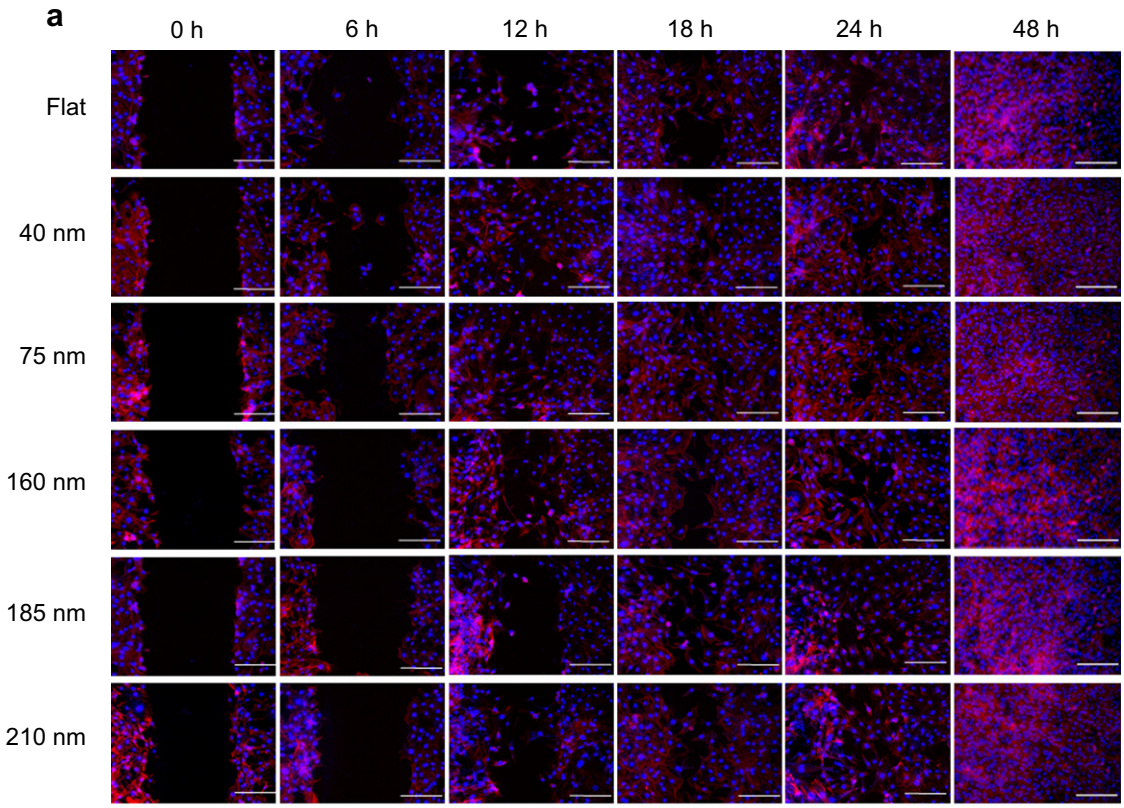

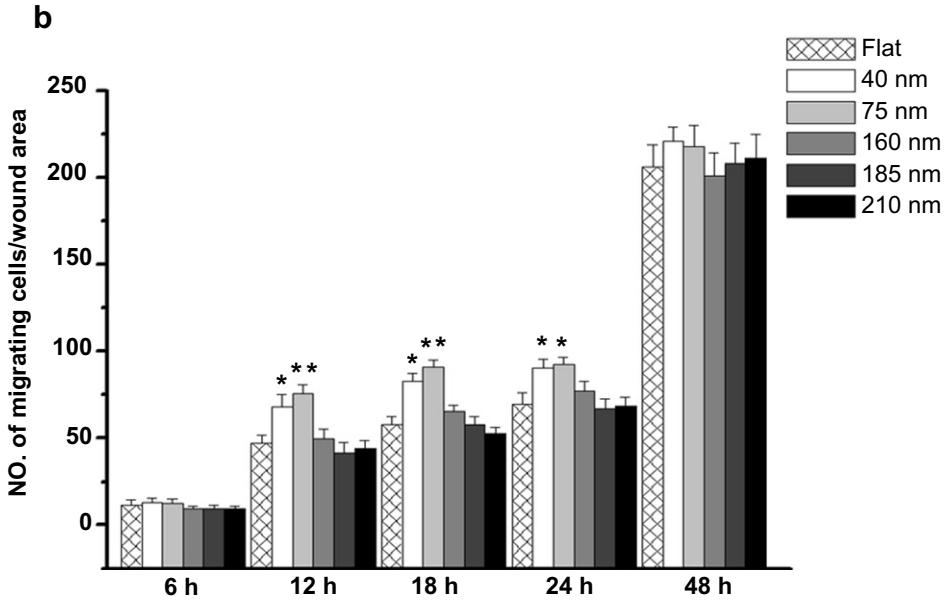

Fig. 9. The migration of fibroblasts on nanopore surfaces in the wound healing assay. (a) Nuclei (blue) and actin filaments (red) were visualised by DAPI and phalloidin staining at 6, 12, 18, 24 and 48 h. (b) The quantification of migrating fibroblasts. The mean ± SD from at least 6 experiments is shown. Scale bar = 200 μm $^{*}p < 0.05$; $^{**}p < 0.01$ when compared with flat control surfaces. (For interpretation of the references to colour in this figure legend, the reader is referred to the web version of this article.)

almost uniformly down-regulated on 400 nm pitch surfaces compared to the behaviour of cells grown on control surfaces [37]. In our study, we noticed differences in integrin gene expression that depended on the stainless steel pore size. Fibroblasts cultured on the 40 or 75 nm nanopore surfaces showed similar integrin expression patterns at 12 and 72 h, and significant variation was observed in the expression of the α2, α9, α11, β3 and β6 subunits within 24 h. Integrins should be spatially and temporally regulated by nanopore surfaces. However, the regulation of the expression of integrins by the nanopore surfaces should be complex. It is well known that ECM production is enhanced on rough nano-patterned surfaces, and at least part of this increase is caused by an increase in

collagen synthesis [19]. Therefore, the adsorption of integrins onto the ECM through various nanoscale pore surfaces should be another factor in determining cell response.

Cell adhesion directly governs cell behaviours by regulating integrins. Integrin αV is known to mediate cell migration, adhesion and survival through binding to ECM proteins [38]. The subunit αV showed increased expression on titanium surfaces with 30 nm nanopores and exhibited an enhanced morphology and facilitated the differentiation of osteoblasts [39]. Previous studies identified that the integrins α2β1, α3β1, α5β1, α5β3, α9β1, α11β1, αVβ3, and αVβ6 are required for cell migration during tissue repair [40–46]. In our study, the gene expressions of integrins such as α2, α9, α11, β3 and β6 were slightly up-regulated on nanopore surfaces with features sizes smaller than 75 nm. According to the western blot results, the production of integrin αV was significantly increased in fibroblasts cultured on 40, 75 and 160 nm nanopores at 72 h. Integrin αV was activated after 72 h and induced the formation of focal adhesions in addition to increasing the cell area and viability of fibroblasts on both the 40 and 75 nm nanopore surfaces. Integrin α2 also plays a critical role in cell motility and adhesion via focal adhesion kinase (FAK) signalling [8]. Previous reports have shown that mice deficient in integrin α2 also show reduced wound healing and fibroblast adhesion [47]. Our findings revealed that integrin α2 expression was significantly induced by the 75 nm and 185–210 nm nanopore surfaces at 12 h and 24 h, respectively. According to cell responses such as focal adhesion and cell migration, integrin α2 may not be required for the initial attachment of cells to surfaces with pores measuring <75 nm. For surfaces with pores measuring >185 nm, fibroblasts expressed integrin α2 at 24 h to adhere to the substrates.

There is a growing body of evidence that ERK signalling, in addition to its role in the control of cell proliferation and adhesion, is also implicated in the regulation of cell motility. The phosphorylation of ERK1/2 has been linked to alterations in focal adhesion formation, and it is known to control cell contraction, thus facilitating cell migration [48]. Previous studies have proposed that the extent of phosphorylation of ERK1/2 is highest in stem cells grown on 15 nm nanotubes and lowest on 100 nm nanotube surfaces [49]. In these studies, significant changes in phosphorylated ERK1/2 were observed in fibroblasts grown on different nanopore structures. Comparing to our work, the <75 nm nanopores hold the ability to induce phosphorylation of ERK1/2. In addition, integrins' control over cell motility via ERK1/2 activation has been proposed [8]. Integrins mediate cell–substrate signalling by activating intracellular FAK and phosphatase signalling to trigger downstream biochemical signals [20]. To make the point more clear, the expression of FAK and phosphorylated FAK (pFAK) was derived from western blot (Fig. S1). Protein analysis indicated that the 40 and 75 nm nanopore surfaces stimulate phosphorylation of FAK in 24 h. The results further confirmed the assumption that the cells on <75 nm nanopores may have higher maturation of adhesions in comparison with >160 nm nanopores. A similar trend for pERK1/2 expression was observed. Vinculin may regulate proliferation and motility via ERK by controlling the accessibility of integrin for FAK interaction. Our results suggest integrin-ERK1/2 signalling in the formation of vinculin and consequent regulation of fibroblast migration.

The ERK pathway has been shown to promote cell adhesion and facilitate the process of cell migration during physiological processes such as wound healing. The acquisition of cell motility is a key property of fibroblast cells in tissue repair. Fibroblast migration enhances wound healing [50]. Previous studies have shown that nanotubes with diameters measuring 50–80 nm enhance cell migration compared to flat Ti surfaces [51]. Nanotubes enhance the cell motility of both MSC and endothelial cells on 15 nm nanotubes [52]. Our results indicated that the 40 and 75 nm nanopore surfaces stimulate the migration of fibroblasts. A similar trend for pERK1/2 expression was also observed. The temporal and spatial expression of pERK1/2 derived from western blotting was consistent with the results of cell migration. Therefore, the regulation of cell motility and migration most likely represents a major mechanism by which the ERK pathway promotes fibroblasts to migrate into wounded regions.

The intracellular mechanisms for topology-mediated cellular functions have not yet been fully addressed. By using nanopore surfaces, we found that topographical cues on a substrate could promote focal adhesion and cytoskeleton organisation to enhance cell migration by integrin and ERK1/2 activation. The modulation of ERK1/2-mediated migration and related cell signalling by nano-patterned surfaces could improve the design of implant surfaces within the fields of biomaterials science and tissue engineering.

5. Conclusion

In the present study, we fabricated 316 L stainless steel substrates with different pore sizes ranging between 40 and 210 nm. The nanoscale pore surfaces are able to influence the expression of integrin and direct cell behaviours such as cell migration, proliferation and focal adhesion formation. Fibroblast attachment and migration are highly promoted by <75 nm nanopore surfaces during initial growth. These nano-patterned surfaces can modulate integrin expression, promote adhesion, and enhance the migration of fibroblasts. In this study, the temporal and spatial modulation of the expression of integrins and ERK1/2 by nanopores was demonstrated. Nanopores may have pivotal regulatory functions in wound healing processes. The obtained results will contribute to the design of functional surfaces that control cell behaviour and improve wound healing for stainless steel implants.

Acknowledgements

This study was supported in part by the National Science Counsel Grant 100-2923-B-009-001-MY3 and by "Aim for the Top University Plan" of the National Chiao Tung University and Ministry of Education, Taiwan, R.O.C.

Appendix A. Supplementary data

Supplementary data related to this article can be found at http://dx.doi.org/10.1016/j.biomaterials.2012.09.078.

References

[1] Vicente-Manzanares M, Choi CK, Horwitz AR. Integrins in cell migration – the actin connection. J Cell Sci 2009;122:199–206.
[2] Sherratt JA, Dallon JC. Theoretical models of wound healing: past successes and future challenges. C R Biol 2002;325:557–64.
[3] Coolen NA, Schouten KCWM, Boekema BKHL, Middelkoop E, Ulrich MMW. Wound healing in a fetal, adult, and scar tissue model: a comparative study. Wound Repair Regen 2010;18:291–301.
[4] Lee JW, Juliano RL. Alpha 5 beta 1 integrin protects intestinal epithelial cells from apoptosis through a phosphatidylinositol 3-kinase and protein kinase B-dependent pathway. Mol Biol Cell 2000;11:1973–87.
[5] Popova SN, Barczyk M, Tiger CF, Beertsen W, Zigrino P, Aszodi A, et al. Alpha 11 beta 1 integrin-dependent regulation of periodontal ligament function in the erupting mouse incisor. Mol Cell Biol 2007;27:4306–16.
[6] Huttenlocher A, Horwitz AR. Integrins in cell migration. Cold Spring Harb Perspect Bio 2011;3:a005074.
[7] Sawhney RS, Sharma B, Humphrey LE, Brattain MG. Integrin α2 and extracellular signal-regulated kinase are functionally linked in highly malignant autocrine transforming growth factor-α-driven colon cancer cells. J Biol Chem 2003;278:19861–9.
[8] Sawhney RS, Cookson MM, Omar Y, Hauser J, Brattain MG. Integrin alpha2-mediated ERK and calpain activation play a critical role in cell adhesion and

motility via focal adhesion kinase signaling: identification of a novel signaling pathway. J Biol Chem 2006;281:8497–510.
[9] Teranishi S, Kimura K, Nishida T. Role of formation of an ERK-FAK-paxillin complex in migration of human corneal epithelial cells during wound closure in vitro. Invest Ophthalmol Vis Sci 2009;12:5464–652.
[10] Cadosch D, Chan E, Gautschi OP, Simmen HP, Filgueira L. Bio-corrosion of stainless steel by osteoclasts-in vitro evidence. J Orthop Res 2009;27:841–6.
[11] Malheiro VN, Spear RL, Brooks RA, Markaki AE. Osteoblast and monocyte responses to 444 ferritic stainless steel intended for a magneto-mechanically actuated fibrous scaffold. Biomaterials 2011;32:6883–92.
[12] Misra RDK, Thein-Han WW, Pesacreta TC, Hasenstein KH, Somani MC, Karjalainen LP. Favorable modulation of pre-osteoblast response to nanograined/ultrafine-grained structures in austenitic stainless steel. Adv Mater 2009;21:1280–5.
[13] Dey A, Nandi SK, Kundu B, Kumar C, Mukherjee P, Roy S, et al. Evaluation of hydroxyapatite and beta-tricalcium phosphate microplasma spray coated pin intra-medullary for bone repair in a rabbit model. Ceram Int 2011;37: 1377–91.
[14] Aparicio C, Rodriguez D, Gil FJ. Variation of roughness and adhesion strength of deposited apatite layers on titanium dental implants. Mat Sci Eng C-mater 2011;31:320–4.
[15] Rokkum M, Reigstad A, Johansson CB, Albrektsson T. Tissue reactions adjacent to well-fixed hydroxyapatite-coated acetabular cups – histopathology of ten specimens retrieved at reoperation after 0.3 to 5.8 years. J Bone Jt Surg Br 2003;85B:440–7.
[16] Oh S, Brammer KS, Li YS, Teng D, Engler AJ, Chien S, et al. Stem cell fate dictated solely by altered nanotube dimension. Proc Natl Acad Sci U S A 2009; 106:2130–5.
[17] Brammer KS, Oh S, Gallagher JO, Jin S. Enhanced cellular mobility guided by TiO_2 nanotube surfaces. Nano Lett 2008;8:786–93.
[18] Lim JY, Dreiss AD, Zhou ZY, Hansen JC, Siedlecki CA, Hengstebeck RW, et al. The regulation of integrin-mediated osteoblast focal adhesion and focal adhesion kinase expression by nanoscale topography. Biomaterials 2007;28: 1787–97.
[19] Olivares-Navarrete R, Raz P, Zhao G, Chen J, Wieland M, Cochran DL, et al. Integrin alpha 2 beta 1 plays a critical role in osteoblast response to micron-scale surface structure and surface energy of titanium substrates. Proc Natl Acad Sci USA 2008;105:15767–72.
[20] Chen W, Villa-Diaz LG, Sun Y, Weng S, Kim JK, Lam RH, et al. Nanotopography influences adhesion, spreading, and self-renewal of human embryonic stem cells. ACS Nano 2012;6:4094–103.
[21] Martin F, Del Frari D, Cousty J, Bataillon C. Self-organisation of nanoscaled pores in anodic oxide overlayer on stainless steels. Electrochim Acta 2009;54: 3086–91.
[22] Cetrullo S, Facchini A, Stanic I, Tantini B, Pignatti C, Caldarera C, et al. Difluoromethylornithine inhibits hypertrophic, pro-fibrotic and pro-apoptotic actions of aldosterone in cardiac cells. Amino Acids 2010;38:525–31.
[23] Forte G, Minieri M, Cossa P, Antenucci D, Sala M, Gnocchi V, et al. Hepatocyte growth factor effects on mesenchymal stem cells: proliferation, migration, and differentiation. Stem Cells 2006;24:23–33.
[24] Pan HA, Hung YC, Su CW, Tai SM, Chen CH, Ko FH, et al. A nanodot array modulates cell adhesion and induces an apoptosis-like abnormality in NIH-3T3 cells. Nanoscale Res Lett 2009;4:903–12.
[25] Zaidel-Bar R, Ballestrem C, Kam Z, Geiger B. Early molecular events in the assembly of matrix adhesions at the leading edge of migrating cells. J Cell Sci 2003;116:4605–13.
[26] Barczyk M, Carracedo S, Gullberg D. Integrins Cell Tissue Res 2010;339:269–80.
[27] Kaverina I, Straube A. Regulation of cell migration by dynamic microtubules. Semin Cell Dev Biol 2011;22:968–74.
[28] Yousaf MN. Model substrates for studies of cell mobility. Curr Opin Chem Biol 2009;13:697–704.
[29] Zhu X, Chen J, Scheideler L, Reichl R, Geis-Gerstorfer J. Effects of topography and composition of titanium surface oxides on osteoblast responses. Biomaterials 2004;25:4087–103.
[30] Hu J, Tian JH, Shi J, Zhang F, He DL, Liu L, et al. Cell culture on AAO nanoporous substrates with and without geometry constrains. Microelectron Eng 2011; 88:1714–7.
[31] Arnold M, Cavalcanti-Adam EA, Glass R, Blummel J, Eck W, Kantlehner M, et al. Activation of integrin function by nanopatterned adhesive interfaces. Chemphyschem 2004;5:383–8.
[32] Huang JH, Grater SV, Corbellinl F, Rinck S, Bock E, Kemkemer R, et al. Impact of order and disorder in RGD nanopatterns on cell adhesion. Nano Lett 2009;9: 1111–6.
[33] Schvartzman M, Palma M, Sable J, Abramson J, Hu X, Sheetz MP, et al. Nanolithographic control of the spatial organization of cellular adhesion receptors at the single-molecule level. Nano Lett 2011;11:1306–12.
[34] Washburn NR, Yamada KM, Simon Jr CG, Kennedy SB, Amis EJ. High-throughput investigation of osteoblast response to polymer crystallinity: influence of nanometer-scale roughness on proliferation. Biomaterials 2004; 25:1215–24.
[35] Schmidt S, Friedl P. Interstitial cell migration: integrin-dependent and alternative adhesion mechanisms. Cell Tissue Res 2010;339:83–92.
[36] Biggs MJP, Richards RG, Dalby MJ. Nanotopographical modification: a regulator of cellular function through focal adhesions. Nanomedicine 2010;6: 619–33.
[37] Gasiorowski JZ, Liliensiek SJ, Russell P, Stephan DA, Nealey PF, Murphy CJ. Alterations in gene expression of human vascular endothelial cells associated with nanotopographic cues. Biomaterials 2010;31:8882–8.
[38] Worth DC, Hodivala-Dilke K, Robinson SD, King SJ, Morton PE, Gertler FB, et al. Alpha v beta 3 integrin spatially regulates VASP and RIAM to control adhesion dynamics and migration. J Cell Biol 2010;189:369–83.
[39] Lavenus S, Berreur M, Trichet V, Pilet P, Louarn G, Layrolle P. Adhesion and osteogenic differentiation of human mesenchymal stem cells on titanium nanopores. Eur Cell Mater 2011;22:84–96.
[40] Erikson DW, Burghardt RC, Bayless KJ, Johnson GA. Secreted phosphoprotein 1 (SPP1, osteopontin) binds to integrin alpha v beta 6 on porcine trophectoderm cells and integrin alpha v beta 3 on uterine luminal epithelial cells, and promotes trophectoderm cell adhesion and migration. Biol Reprod 2009;81: 814–25.
[41] Eslami A, Gallant-Behm CL, Hart DA, Wiebe C, Honardoust D, Gardner H, et al. Expression of integrin alpha v beta 6 and TGF-beta in scarless vs scar-forming wound healing. J Histochem Cytochem 2009;57:543–57.
[42] Lobert VH, Brech A, Pedersen NM, Wesche J, Oppelt A, Malerod L, et al. Ubiquitination of alpha 5 beta 1 integrin controls fibroblast migration through lysosomal degradation of fibronectin-integrin complexes. Dev Cell 2010;19: 148–59.
[43] Pezzatini S, Morbidelli L, Solito R, Paccagnini E, Boanini E, Bigi A, et al. Nanostructured HA crystals up-regulate FGF-2 expression and activity in microvascular endothelium promoting angiogenesis. Bone 2007;41:523–34.
[44] Reynolds LE, Conti FJ, Silva R, Robinson SD, Iyer V, Rudling R, et al. Alpha 3 beta 1 integrin-controlled Smad7 regulates reepithelialization during wound healing in mice. J Clin Invest 2008;118:965–74.
[45] Sadok A, Pierres A, Dahan L, Prevot C, Lehmann M, Kovacic H. NADPH Oxidase 1 controls the persistence of directed cell migration by a rho-dependent switch of alpha 2/alpha 3 integrins. Mol Cell Biol 2009;29:3915–28.
[46] Singh P, Chen C, Pal-Ghosh S, Stepp MA, Sheppard D, Van De Water L. loss of integrin alpha 9 beta 1 results in defects in proliferation, causing poor re-epithelialization during cutaneous wound healing. J Invest Dermatol 2009; 129:217–28.
[47] Takada Y, Ye XJ, Simon S. The integrins. Genome Biol 2007;8:215.
[48] Webb DJ, Donais K, Whitmore LA, Thomas SM, Turner CE, Parsons JT, et al. FAK-Src signalling through paxillin, ERK and MLCK regulates adhesion disassembly. Nat Cell Biol 2004;6:154–61.
[49] Park J, Bauer S, von der Mark K, Schmuki P. Nanosize and vitality: TiO_2 nanotube diameter directs cell fate. Nano Lett 2007;7:1686–91.
[50] Jeon YK, Jang YH, Yoo DR, Kim SN, Lee SK, Nam MJ. Mesenchymal stem cells' interaction with skin: wound-healing effect on fibroblast cells and skin tissue. Wound Repair Regen 2010;18:655–61.
[51] Arnold M, Hirschfeld-Warneken VC, Lohmuller T, Heil P, Blummel J, Cavalcanti-Adam EA, et al. Induction of cell polarization and migration by a gradient of nanoscale variations in adhesive ligand spacing. Nano Lett 2008; 8:2063–9.
[52] Park J, Bauer S, Schmuki P, von der Mark K. Narrow window in nanoscale dependent activation of endothelial cell growth and differentiation on TiO_2 nanotube surfaces. Nano Lett 2009;9:3157–64.